



Core structure of static ferrodark solitons in a spin-1 Bose-Einstein condensate

Xiaoquan Yu ^{1,2,*} and P. B. Blakie ²

¹Graduate School of China Academy of Engineering Physics, Beijing 100193, China

²Department of Physics, Centre for Quantum Science, and Dodd-Walls Centre for Photonic and Quantum Technologies, University of Otago, Dunedin 9016, New Zealand



(Received 4 April 2022; accepted 23 June 2022; published 18 July 2022)

We develop an analytical description of static ferrodark solitons, the \mathbb{Z}_2 topological defects in the magnetic order, in the easy-plane phase of ferromagnetic spin-1 Bose-Einstein condensates. We find that the type-I ferrodark soliton has a single width while the type-II ferrodark soliton exhibits two characteristic length scales. The proposed *Ansätze* show excellent agreement with numerical results. Spin-singlet amplitudes, nematic tensor densities, and nematic currents of ferrodark solitons are also discussed. The \mathbb{Z}_2 topological defects in the mass superfluid order, dark-dark-dark vector solitons, are obtained exactly in the parameter regime where exact ferrodark solitons exist. The dark-dark-dark vector soliton has higher excitation energy than ferrodark solitons.

DOI: [10.1103/PhysRevResearch.4.033056](https://doi.org/10.1103/PhysRevResearch.4.033056)

I. INTRODUCTION

A spin-1 Bose-Einstein condensate (BEC) is a coherent state constituted by atoms occupying hyperfine spin levels $|F = 1, m = +1, 0, -1\rangle$ that interact via spin-mixing collisions, exhibiting superfluidity and magnetic orders [1–6]. This spinor superfluid supports topological excitations that are absent in scalar and two-component BECs, adding novel features to phenomena such as the Berezinskii-Kosterlitz-Thouless transitions [7,8] and out-of-equilibrium processes in superfluids, including Kibble-Zurek mechanism [9,10], phase ordering [11–17], and thermalization processes [18,19]. It also provides additional to magnetic thin films, a prominent platform for exploring quantum magnetism.

In the presence of a magnetic field along the z axis, the ground state of a ferromagnetic spin-1 BEC can be in the easy-axis or broken-axisymmetry ferromagnetic phases, or the nonmagnetized polar phase, each separated by a quantum phase transition [5,6]. The easy-plane phase, being the broken-axisymmetry phase with the magnetization lying in the xy plane, is particularly interesting as it describes XY magnetism and supports various unique topological excitations [20–23]. A substantial amount of work has been devoted to studying quenches from the polar phase to the easy-plane phase by a change in the magnetic field [4,10,11,13,24–27]. Here polar core vortices are the relevant topological defects in two dimensions (2D) and determine the Kibble-Zurek scaling and the universal dynamic scaling in phase ordering at late times [13]. Domain wall structures also appear in the

early stage of quenches due to the linear instability, but these domain walls are transient and continually decay to polar core vortices [24]. In one dimension (1D), domain walls/solitons are relevant defects and contribute the Kibble-Zurek scalings [9,10] and may play an important role in determining the universal scaling behaviors at later times of the quench [26,27] (i.e., the so-called nonthermal fixed point). However, little is known on the properties of the relevant domain walls/solitons in ferromagnetic spin-1 condensates.

An important question is what topological excitations are supported in the easy-plane phase of ferromagnetic spin-1 BECs? Here the term “topological” refers to the winding number (2D) or the topological charge (1D) of the order parameter being nonzero. In a scalar BEC, vortices (2D) and dark solitons (1D) are the relevant topological excitations. In ferromagnetic spin-1 BECs, the magnetization serves as the local order parameter and quantifies the magnetic order associated with the $SO(3)$ rotational symmetry breaking. In the easy-plane phase, the spin vortices [defects associated with the continuous $SO(2)$ symmetry] are polar core vortices and Mermin-Ho vortices [5,6,28,29], while kinks in the transverse magnetization (defects associated with the discrete \mathbb{Z}_2 symmetry) have been uncovered only recently thanks to the discovery of ferrodark solitons (FDSs) (also referred to as magnetic domain walls) [22,23]. The FDSs are magnetic kinks that connect transverse magnetic domains with opposite magnetizations, signified by the magnetization \mathbf{F} vanishing at the core and changing its sign across the core. The superfluid density n has a dip but does not vanish at the core. The FDSs have two types and exhibit several distinct features, including positive inertial mass, stability against snake deformations, and oscillations in a linear potential due to the transition between the two types at the maximum speed [22,23]. The static profiles of FDSs have been studied in detail when $q \rightarrow 0$ [22], where q is the quadratic Zeeman energy of the atom in the magnetic field. However, at finite q , except for exactly solvable cases [22,23], the core structure of FDSs remain unexplored.

*xqyu@gscaep.ac.cn

Published by the American Physical Society under the terms of the [Creative Commons Attribution 4.0 International license](https://creativecommons.org/licenses/by/4.0/). Further distribution of this work must maintain attribution to the author(s) and the published article's title, journal citation, and DOI.

In this paper we study the core structure of static FDSs for finite quadratic Zeeman energies ($q > 0$) in the whole easy-plane phase. Accurate *Ansätze* are proposed and show good agreement with numerical results. In particular, we obtain the characteristic length scales analytically via consistent asymptotic analysis, finding that type-I FDS has a single length scale while type-II FDS requires two length scales to describe the width near the core and the width away from the core, respectively. Spin-singlet amplitudes, nematic tensor densities, and nematic currents of FDSs exhibit rich structure and provide a complete description of static FDSs. The dark-dark-dark vector solitons, which are the \mathbb{Z}_2 topological defects in the mass superfluid order, are also discussed.

II. SPIN-1 BECs

The mean-field Hamiltonian density of a spin-1 condensate reads

$$\mathcal{H} = \frac{\hbar^2 |\nabla \psi|^2}{2M} + \frac{g_n}{2} |\psi^\dagger \psi|^2 + \frac{g_s}{2} |\psi^\dagger \mathbf{S} \psi|^2 + q \psi^\dagger S_z^2 \psi, \quad (1)$$

where the three-component wave function $\psi = (\psi_{+1}, \psi_0, \psi_{-1})^T$ describes the coherent atomic field in the three atomic hyperfine states $|F=1, m=+1, 0, -1\rangle$, M is the atomic mass, $g_n > 0$ is the density-dependent interaction strength, g_s is the spin-dependent interaction strength, and $S_{j=x,y,z}$ are the spin-1 matrices $[\mathbf{S} = (S_x, S_y, S_z)]$ [5,6]. The spin-dependent interaction terms describe spin-mixing collisions: $|00\rangle \leftrightarrow |+1\rangle|-1\rangle$, originating from the spin dependence of the s -wave collisions [5]. The magnetic field is along the z axis and q denotes the quadratic Zeeman energy.

At the mean-field level, the dynamics of the field ψ is governed by the spin-1 Gross-Pitaevskii equations (GPEs) which are obtained via the canonical equation $\partial \psi_m / \partial t = \delta \mathcal{H} / \delta (i \hbar \psi_m^*)$:

$$i \hbar \frac{\partial \psi_{\pm 1}}{\partial t} = [H_0 + g_s(n_0 + n_{\pm 1} - n_{\mp 1}) + q] \psi_{\pm 1} + g_s \psi_0^2 \psi_{\mp 1}^*, \quad (2)$$

$$i \hbar \frac{\partial \psi_0}{\partial t} = [H_0 + g_s(n_{+1} + n_{-1})] \psi_0 + 2g_s \psi_0^* \psi_{+1} \psi_{-1}, \quad (3)$$

where $H_0 = -\hbar^2 \nabla^2 / 2M + g_n n$, $n = \sum n_m$ is the total number density and $n_m = |\psi_m|^2$ is the component density.

A distinguishing feature of spin-1 BECs is that the system supports magnetic orders, with the magnetization $\mathbf{F} \equiv \psi^\dagger \mathbf{S} \psi = (F_x, F_y, F_z)$ serving as the local order parameter. Here

$$F_x = \psi^\dagger S_x \psi = \frac{1}{\sqrt{2}} [\psi_0^* (\psi_{+1} + \psi_{-1}) + \text{H.c.}], \quad (4)$$

$$F_y = \psi^\dagger S_y \psi = \frac{i}{\sqrt{2}} [\psi_0^* (\psi_{+1} - \psi_{-1}) - \text{H.c.}], \quad (5)$$

$$F_z = \psi^\dagger S_z \psi = |\psi_{+1}|^2 - |\psi_{-1}|^2. \quad (6)$$

It is convenient to introduce the transverse magnetization as the complex density

$$F_\perp \equiv F_x + i F_y = \sqrt{2} (\psi_0 \psi_{+1}^* + \psi_0^* \psi_{-1}). \quad (7)$$

For ferromagnetic coupling $g_s < 0$ (^{87}Rb , ^7Li), $|\mathbf{F}| > 0$ and for antiferromagnetic coupling $g_s > 0$ (^{23}Na), $\mathbf{F} = 0$. At $q = 0$, the system processes $\text{SO}(3)$ rotational symmetry and the total magnetization $\mathbf{M} = \int d\mathbf{r} \mathbf{F}$ is conserved. In the presence of a magnetic field ($q \neq 0$), the remaining symmetry is $\text{SO}(2)$ rotational symmetry, and yields to the conservation of the total magnetization along the z axis $M_z = \int d\mathbf{r} F_z$. In contrast to binary BECs, a spin-1 BEC is not an incoherent mixture of condensates, i.e., the system does not process $\text{U}(1) \times \text{U}(1) \times \text{U}(1)$ symmetry [5].

III. EASY-PLANE PHASE

For a uniform ferromagnetic system ($g_s < 0$) with total density n_b , the energy density is

$$\mathcal{H} = \frac{1}{2} g_n n_b^2 + \frac{g_s}{2} |\mathbf{F}|^2 + q(n_b - n_0). \quad (8)$$

The uniform ground state is found by minimizing the free energy density $\mathcal{F} \equiv \mathcal{H} - p F_z$ [3,30], where p is the Lagrange multiplier. In the following we only consider $F_z = 0$. Hence for $q > 0$ the magnetization prefers to lie in the transverse plane, realizing an easy-plane ferromagnetic phase [5,6]. Plugging the wave function

$$\psi = (\sqrt{n_{+1}} e^{i\theta_{+1}}, \sqrt{n_0} e^{i\theta_0}, \sqrt{n_{-1}} e^{i\theta_{-1}})^T \quad (9)$$

into the energy function Eq. (8), we obtain

$$E = 2g_s n_0 (n_b - n_0) \cos^2 \left[\theta_0 - \frac{\theta_{+1} + \theta_{-1}}{2} \right] + \frac{g_n}{2} n_b^2 + q(n_b - n_0). \quad (10)$$

The energy E reaches the minimum when

$$2\theta_0 = \theta_{+1} + \theta_{-1}, \quad (11)$$

$$n_0 = n_0^g = \frac{n_b(1 + \tilde{q})}{2}, \quad (12)$$

$$n_{\pm 1} = n_{\pm 1}^g = \frac{n_b(1 - \tilde{q})}{4}, \quad (13)$$

where $\tilde{q} \equiv -q/(2g_s n_b)$. The ground-state magnetization reads

$$F_\perp^g(\tau) = n_b \sqrt{1 - \tilde{q}^2} e^{i\tau}, \quad (14)$$

where $\tau = \theta_0 - \theta_{+1} = \theta_{-1} - \theta_0$ describes the orientation of the transverse magnetization [the $\text{SO}(2)$ rotational angle about the z axis ($e^{-i\tau S_z}$)], quantifying the magnetic order. The ground wave function can be written as

$$\psi^g(\theta, \tau) = \sqrt{n_b} e^{i\theta} e^{-i\tau S_z} \left(\sqrt{\frac{n_{+1}^g}{n_b}}, \sqrt{\frac{n_0^g}{n_b}}, \sqrt{\frac{n_{-1}^g}{n_b}} \right)^T, \quad (15)$$

where θ describes the global $\text{U}(1)$ phase and quantifies the mass superfluid order. Note that the choice of the global phase θ is not unique and depends on the realization of the spin rotation in spin states. For instance, for the state $e^{i\theta_0} (\sqrt{n_{+1}^g} e^{-i\tau}, \sqrt{n_0^g}, \sqrt{n_{-1}^g} e^{i\tau})^T$, θ_0 can be regarded as the global phase. Rearranging the phases in spin states, it becomes $e^{i\theta_{+1}} (\sqrt{n_{+1}^g}, \sqrt{n_0^g} e^{i\tau}, \sqrt{n_{-1}^g} e^{2\tau i})^T$ and then $\theta = \theta_{+1}$.

The positiveness of component densities $n_{\pm 1}$ requires $q < -2g_s n_b$ which sets the parameter range of the easy-plane

phase. Note that for $q < 0$, under the constraint $M_z = 0$, a fragmented state of mixed $F_z = n_b$ and $F_z = -n_b$ domains has lower energy than any uniform state [5,6].

IV. \mathbb{Z}_2 TOPOLOGICAL DEFECTS

In this section, we discuss \mathbb{Z}_2 topological defects in the easy-plane phase of a ferromagnetic BEC. Hereafter we consider 1D systems. It is useful to introduce the topological charge to characterize \mathbb{Z}_2 defects in the magnetic order

$$Q_{F_\perp} = \frac{1}{2|F_\perp^g|} \int_{-\infty}^{\infty} dx \partial_x F_\perp(x) \tag{16}$$

and the topological charge to characterize \mathbb{Z}_2 defects in the mass superfluid order

$$Q_\psi = \prod_{m=-1,0,1} Q_{\psi_m}, \tag{17}$$

where

$$Q_{\psi_m} = \frac{1}{2|\psi_m^g|} \int_{-\infty}^{\infty} dx \partial_x \psi_m(x). \tag{18}$$

The topological charges can be also expressed in terms of relevant phases:

$$Q_{F_\perp} = \frac{1}{\pi} \int_{-\infty}^{\infty} dx \partial_x \tau(x) \tag{19}$$

and

$$Q_\psi = \frac{1}{\pi} \int_{-\infty}^{\infty} dx \partial_x \theta(x). \tag{20}$$

It should be understood that here the results are modulo 2. The SO(2) spin rotation $e^{-i\pi S_z}$ and the U(1) gauge transformation $e^{-i\pi}$ play the role of charge conjugation operators and change signs of Q_{F_\perp} and Q_ψ , respectively. Note that the spin rotation $e^{-i\pi S_z}$ does not change the sign of Q_ψ and the gauge transformation $e^{-i\pi}$ keeps the sign of Q_{F_\perp} unchanged.

A. \mathbb{Z}_2 defects in the magnetic order: Ferrodark solitons

Let us consider two oppositely magnetized domains with $\tau = 0$ and $\tau = \pi$, respectively, and search for a magnetic kink $F_\perp(x)$ that interpolates the two domains, namely,

$$F_\perp(-\infty) = F_\perp^g(\pi) \text{ and } F_\perp(+\infty) = F_\perp^g(0) = -F_\perp(-\infty). \tag{21}$$

It was found that an Ising-type magnetic kink satisfies the condition Eq. (21), signified by F_\perp vanishing at the core and changing its sign across the core. This kink was referred to as FDS [23]. Exact FDS solutions of Eqs. (2) and (3) were found at $g_s = -g_n/2$ [22,23]:

$$F_\perp^{I,II}(x) = |F_\perp^g| \tanh\left(\frac{x}{2\ell_{\text{ex}}^{I,II}}\right), \tag{22}$$

$$n^{I,II}(x) = n_b \left[1 - \frac{(1 \mp \tilde{q})}{2} \text{sech}^2\left(\frac{x}{2\ell_{\text{ex}}^{I,II}}\right) \right], \tag{23}$$

where $\ell_{\text{ex}}^{I,II} = \hbar/\sqrt{2g_n n_b M(1 \mp \tilde{q})}$, and the minus and plus signs in front of q are referred to as type-I and type-II FDSs,

respectively. Note that $\ell_{\text{ex}}^{II} \leq \ell_{\text{ex}}^I$ with the equality holding at $q = 0$. The corresponding wave functions read

$$\psi_{\pm 1}^I(x) = \sqrt{n_{\pm 1}^g} \tanh\left(\frac{x}{2\ell_{\text{ex}}^I}\right), \quad \psi_0^I(x) = \sqrt{n_0^g} \tag{24}$$

and

$$\psi_{\pm 1}^{II}(x) = \sqrt{n_{\pm 1}^g}, \quad \psi_0^{II}(x) = \sqrt{n_0^g} \tanh\left(\frac{x}{2\ell_{\text{ex}}^{II}}\right). \tag{25}$$

At the core ($x = 0$), the magnetization vanishes [$F_\perp^{I,II}(0) = 0$] while the superfluid density n is finite [$n^{I,II}(0) \neq 0$]. FDSs are topological defects in the magnetic order but not in the superfluid order, namely, $Q_{F_\perp} = \pm 1$ [$Q_{F_\perp} = -1$ for anti-FDSs $e^{-i\pi S_z} \psi^{I,II}(x)$] while $Q_\psi = 0$.

The wave functions of FDSs Eqs. (24) and (25) can be written as follows:

$$\psi^I(x) = [|\psi_{+1}^I|e^{-i\tau(x)}, |\psi_0^I|, |\psi_{-1}^I|e^{i\tau(x)}]^T, \tag{26}$$

$$\psi^{II}(x) = [|\psi_{+1}^{II}|, |\psi_0^{II}|e^{i\tau(x)}, |\psi_{-1}^{II}|e^{i2\tau(x)}]^T, \tag{27}$$

where $\tau(x)$ is a step function: $\tau(x < 0) = -\pi$ and $\tau(x \geq 0) = 0$. Hence type-I and type-II FDSs might be viewed as 1D analogies of polar core vortices and Mermin-Ho vortices, respectively.

We consider stationary excitations which satisfy $\psi_{+1} = \psi_{-1}$ [upon a SO(2) spin rotation] and the stationary GPEs become

$$0 = \left[-\frac{\hbar^2}{2M} \frac{d^2}{dx^2} - \mu + 2g_n n_{\pm 1} + (g_n + 2g_s)n_0 + q \right] \psi_{\pm 1}, \tag{28}$$

$$0 = \left[-\frac{\hbar^2}{2M} \frac{d^2}{dx^2} - \mu + g_n n_0 + 2(g_n + 2g_s)n_{\pm 1} \right] \psi_0, \tag{29}$$

where the chemical potential $\mu = (g_n + g_s)n_b + q/2$ and the wave functions ψ_m are chosen to be real. Clearly U(1) gauge transformations and SO(2) spin rotations keep Eqs. (28) and (29) unchanged. At $g_s = -g_n/2$, Eqs. (28) and (29) become decoupled and admit exact type-I [Eq. (24)] and type-II [Eq. (25)] solutions. It is worth mentioning that the exactly solvable point is within the scope of a ^7Li spin-1 BEC which has been prepared in a regime with a strong spin-dependent interaction [31].

B. \mathbb{Z}_2 defects in the mass superfluid order: Dark-dark-dark vector solitons

There is another soliton solution $\psi(x)$ to the Eqs. (28) and (29) that satisfies

$$\psi(-\infty) = \psi^g(\pi, \tau) \text{ and } \psi(+\infty) = \psi^g(0, \tau) = -\psi(-\infty), \tag{30}$$

and at $g_s = -g_n/2$:

$$\psi_{\pm 1}^d(x) = \sqrt{n_{\pm 1}^g} \tanh\left(\frac{x}{2\ell_{\text{ex}}^d}\right), \quad \psi_0^d(x) = \sqrt{n_0^g} \tanh\left(\frac{x}{2\ell_{\text{ex}}^d}\right). \tag{31}$$

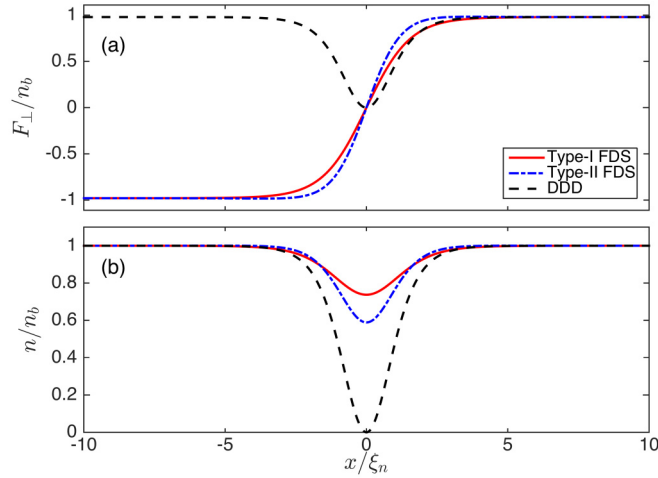


FIG. 1. The transverse magnetization (a) and the density (b) of FDSs and the DDD at $g_s = -0.3g_n$ and $\tilde{q} = 0.2$. Here $\xi_n = \hbar/\sqrt{n_b g_n M}$.

Here we have chosen that $\tau = 0$. The corresponding transverse magnetization and the total density read

$$F_{\perp}^d(x) = |F_{\perp}^s| \tanh\left(\frac{x}{2\ell_{\text{ex}}^{\text{I}}}\right) \tanh\left(\frac{x}{2\ell_{\text{ex}}^{\text{II}}}\right), \quad (32)$$

$$n^d(x) = n^b \left[1 - \frac{1 - \tilde{q}}{2} \text{sech}\left(\frac{x}{2\ell_{\text{ex}}^{\text{I}}}\right)^2 - \frac{1 + \tilde{q}}{2} \text{sech}\left(\frac{x}{2\ell_{\text{ex}}^{\text{II}}}\right)^2 \right]. \quad (33)$$

In the literature this soliton has been referred to as the dark-dark-dark (DDD) vector soliton [32]. The DDD vector soliton is the \mathbb{Z}_2 topological defect in the mass superfluid order, characterized by changing sign of $\psi^d(x)$ across the core [accompanied by $n^d(0) = 0$] and $Q_{\psi} = 1$ [$Q_{\psi} = -1$ for the anti-DDD $e^{-i\pi} \psi^d(x)$]. The DDD vector soliton is not a topological defect in the magnetic order as the transverse magnetization F_{\perp}^d does not change sign across the core [although $F_{\perp}^d(0) = 0$] and $Q_{F_{\perp}} = 0$. Note that the spin rotation $e^{-i\pi S_z}$ does not change the sign of Q_{ψ} , i.e., $Q_{\psi} = 1$ for $e^{-i\pi S_z} \psi^d(x)$ and $Q_{\psi} = -1$ for $e^{-i\pi S_z} e^{-i\pi} \psi^d(x)$. Typical profiles of FDSs and the DDD vector soliton are shown in Fig. 1.

The energy of a DDD vector soliton is higher than a FDS in the parameter region where the DDD vector soliton is supported [33] (see Fig. 2). Here the numerical solutions are obtained using a gradient flow method [34,35]. We quantify the soliton energy as the excess grand canonical energy over that of the ground state, i.e., as $\delta K \equiv K[\psi] - K_g$, where

$$K[\psi] = \int dx (\mathcal{H}[\psi] - \mu n_b) \quad (34)$$

and

$$K_g = \int dx (\mathcal{H}[\psi^g] - \mu n_b) = \frac{n_b^2 [g_s (\tilde{q}^2 - 1) - g_n]}{2} L. \quad (35)$$

Here L is the system size. In the following, we focus on analyzing the core structure of FDSs away from the exactly solvable regime.

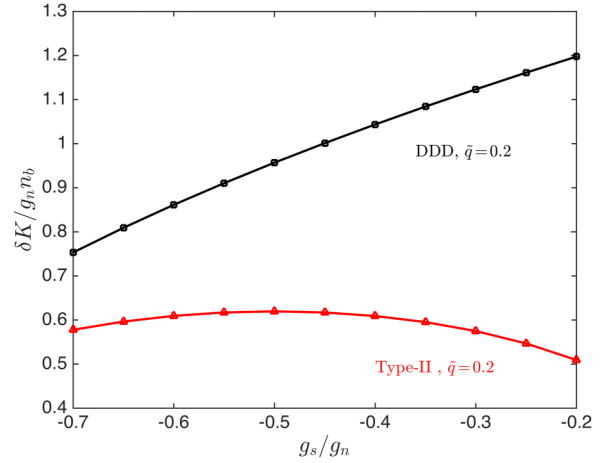


FIG. 2. Numerical results for the energies of type-II FDSs (red triangles) and DDD solitons (black squares) at $\tilde{q} = 0.2$. Here only the type-II FDS energy curve is presented as the type-I FDS always has lower energy (see Sec. V C).

V. CORE STRUCTURE FOR A FINITE QUADRATIC ZEEMAN SHIFT

The fundamental properties of FDSs do not qualitatively change away from the exactly solvable regime ($g_s/g_n = -1/2$, $0 < q < -2g_s n_b$). However, the characteristic length scales do vary as g_s changes and have been characterized in the $q \rightarrow 0$ limit in Ref. [22]. This limit allows us to connect, through $\text{SO}(3)$ spin rotations, various different degenerate forms of the FDS. At $q = 0$, the core structure was conveniently analyzed using a particular rotated state referred to as the sine-Gordon representation. For $q > 0$, the $\text{SO}(3)$ symmetry is broken by the magnetic field and the sine-Gordon-like solitons are no longer stationary solutions [22]. A different scheme is therefore required to obtain the widths of FDSs.

A. Type-I FDSs

Away from the exactly solvable regime, we propose the following *Ansatz* for type-I FDSs:

$$\psi_{\pm 1}^{\text{I}}(x) = \sqrt{n_{\pm 1}^g} \tanh\left(\frac{x}{2\ell^{\text{I}}}\right), \quad (36)$$

$$\psi_0^{\text{I}}(x) = \frac{c^{\text{I}}}{g^{\text{I}} + \cosh\left(\frac{x}{\ell^{\text{I}}}\right)} + \sqrt{n_0^g}, \quad (37)$$

where ℓ^{I} is a length scale describing the core size and g^{I} is introduced to adjust the core structure. For $x \gg \ell^{\text{I}}$, $\psi_{\pm 1}^{\text{I}}(x) \sim \sqrt{n_{\pm 1}^g} (1 - 2e^{-x/\ell^{\text{I}}})$ and $\psi_0^{\text{I}}(x) \sim 2c^{\text{I}} e^{-x/\ell^{\text{I}}} + \sqrt{n_0^g}$. This *Ansatz* solves Eqs. (28) and (29) asymptotically ($x \gg \ell^{\text{I}}$) if ℓ^{I} is a physically acceptable (real and positive) root of the polynomial equation

$$4M^2(g_n + g_s)(4g_s^2 n_b - q^2)y^4 + 4g_n g_s M n_b \hbar^2 y^2 - g_s \hbar^4 = 0 \quad (38)$$

and

$$c^{\text{I}} = -\frac{(g_n + 2g_s)(2g_s n_b + q)\sqrt{2n_b - \frac{q}{g_s}}}{4\sqrt{g_s [g_s n_b^2 (g_n + 2g_s)^2 - q^2 (g_n + g_s)]} + 2g_n q}. \quad (39)$$

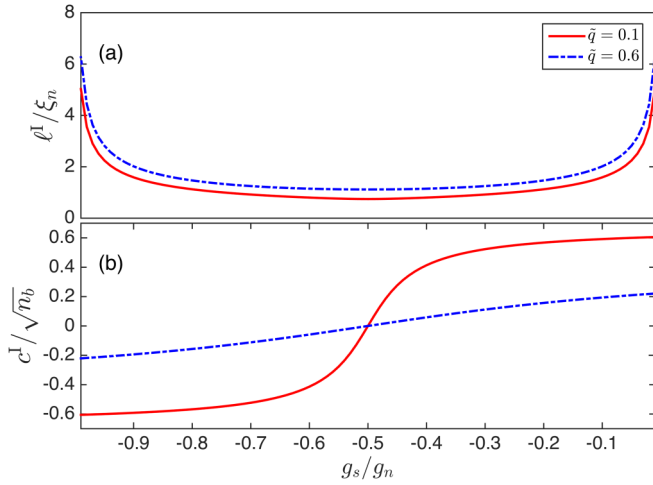


FIG. 3. Key parameters in the *Ansatz* of type-I FDSs given in Eqs. (36) and (37) as functions of g_s for $\tilde{q} = 0.1$ and $\tilde{q} = 0.6$.

Two positive roots of Eq. (38) are

$$y_{\pm} = \frac{g_s \hbar^2}{\sqrt{2M(g_n g_s n_b \pm \sqrt{g_s [g_s n_b^2 (g_n + 2g_s)^2 - q^2 (g_n + g_s)]}}}. \quad (40)$$

It is easy to check that $y_+|_{g_s=-g_n/2} = \ell_{\text{ex}}^I$ [where ℓ_{ex}^I was introduced after Eq. (23)], hence we identify

$$\ell^I = y_+. \quad (41)$$

As $g_s \rightarrow -g_n/2$, $c^I \rightarrow 0$. Moreover c^I changes the sign when g_s crosses the exactly solvable point $-g_n/2$ [Fig. 3(b)], inducing a hump or dip in ψ_0 [Figs. 4(d) and 4(d')].

Near the core $x \sim 0$, solving Eqs. (28) and (29) to leading order, we obtain

$$g_n \left(\frac{c^I}{g^I + 1} + d \right)^3 - \mu \left(\frac{c^I}{g^I + 1} + d \right) + \frac{2c^I \hbar^2}{4(g^I + 1)^2 (\ell^I)^2 M} = 0, \quad (42)$$

which determines the value of g^I . Neglecting the last term of Eq. (42), we obtain

$$g^I = \frac{c^I}{\sqrt{\mu/g_n} - \sqrt{n_0^g}} - 1. \quad (43)$$

Evaluating the last term in Eq. (42) using the result in Eq. (43) verifies that it is small, justifying the approximation used here.

The results in Fig. 4 compare the *Ansatz* in Eqs. (36) and (37) against numerical solution of the GPEs. This comparison shows that the *Ansatz* we have developed provides a very good description of the core structure of the soliton over a wide range of parameters.

B. Type-II FDSs

At the exactly solvable point Eqs. (28) and (29) admit another exact solution—the type-II soliton given in Eq. (25). Away from the exactly solvable point, the core structure of type-II FDSs exhibits additional complexity which requires

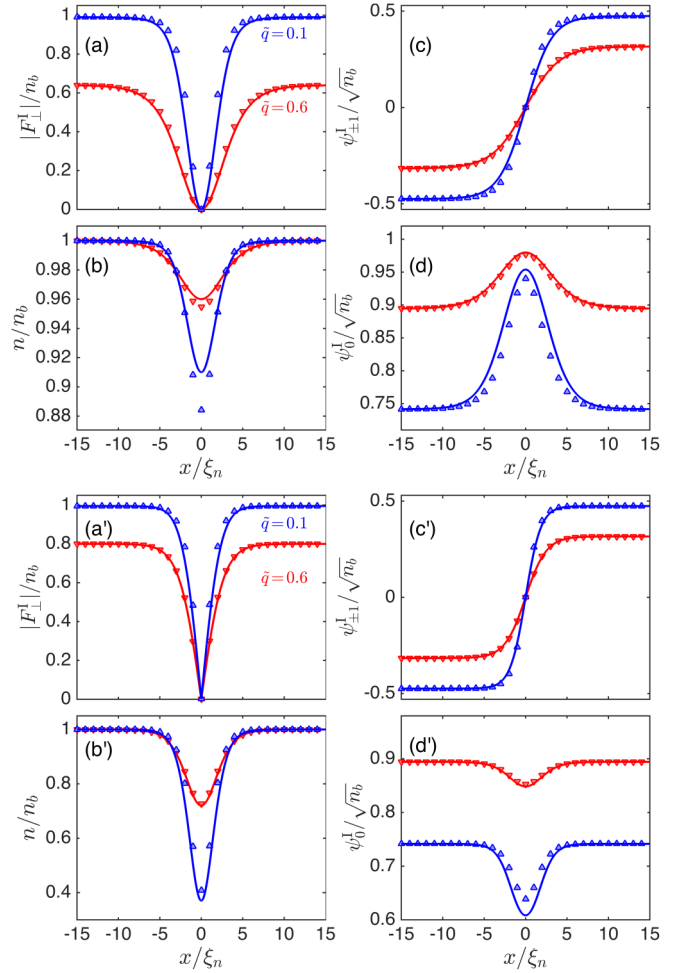


FIG. 4. A comparison between analytical predictions of type-I FDSs (solid lines) and numerical results (markers) at $\tilde{q} = 0.1$ and $\tilde{q} = 0.6$. (a), (b), (c), and (d) are for $g_s/g_n = -0.1$; (a'), (b'), (c'), and (d') are for $g_s/g_n = -0.7$.

two length scales to describe the core widths near and away from the center. We hence propose the following *Ansatz*:

$$\psi_0^{\text{II}}(x) = \sqrt{n_0^g} \tanh\left(\frac{x}{2\ell_a^{\text{II}}}\right) \left(\frac{c^{\text{II}}/\kappa}{\cosh\left(\frac{x}{\ell_b^{\text{II}}}\right)} + 1 \right), \quad (44)$$

$$\psi_{\pm 1}^{\text{II}}(x) = \frac{c^{\text{II}}}{\cosh\left(\frac{x}{\ell_b^{\text{II}}}\right)} + \sqrt{n_{\pm 1}^g}, \quad (45)$$

where we assume $\ell_b^{\text{II}} > \ell_a^{\text{II}}$. For $x \gg \ell_b^{\text{II}}$, $\psi_0^{\text{II}}(x) \sim \sqrt{n_0^g} [1 + 2(c^{\text{II}}/\kappa)e^{-x/\ell_b^{\text{II}}}]$ and $\psi_{\pm 1}^{\text{II}}(x) \sim \sqrt{n_{\pm 1}^g} + 2c^{\text{II}}e^{-x/\ell_b^{\text{II}}}$. Solving Eqs. (28) and (29) asymptotically, we obtain that ℓ_b^{II} has to be a root of Eq. (38) and

$$\kappa = \frac{g_n q - 2g_s \sqrt{n_b^2 (g_n + 2g_s)^2 - \frac{q^2 (g_n + g_s)}{g_s}}}{2g_s (g_n + 2g_s) \sqrt{\frac{2q}{g_s} + 4n_b}}. \quad (46)$$

If the core was characterized by a single length scale, the value of ℓ_b^{II} could be easily set to be y_+ , as it gives rise to the right value at the exactly solvable point, namely, $y_+|_{g_s=-g_n/2} = \ell_{\text{ex}}^{\text{II}}$. However, when the other length scale ℓ_a^{II} is introduced, a

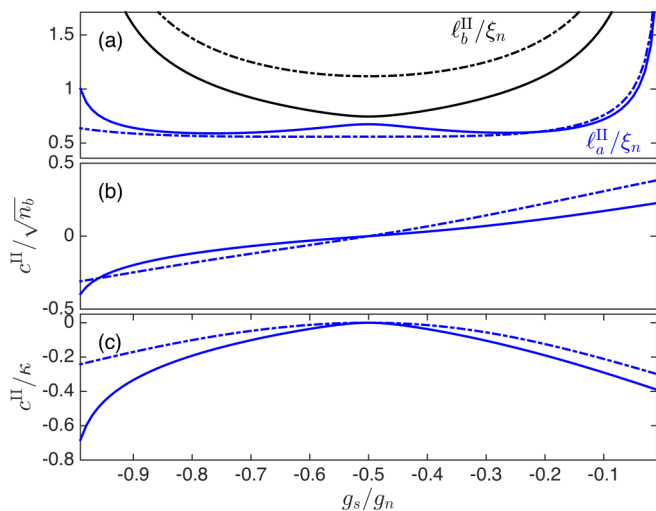


FIG. 5. Key parameters in the *Ansatz* of type-II FDSs [Eqs. (44) and (45)] as functions of g_s for $\tilde{q} = 0.1$ (solid lines) and $\tilde{q} = 0.6$ (dash-dotted lines).

different scenario becomes possible to connect to the exactly solvable point, i.e., $c^{\text{II}} \rightarrow 0$ and $\ell_a^{\text{II}} \rightarrow \ell_{\text{ex}}^{\text{II}}$ as $g_s \rightarrow -g_n/2$. The appropriate choice for ℓ_b^{II} to provide a consistent solution is

$$\ell_b^{\text{II}} = y_- = \ell^{\text{I}}. \quad (47)$$

Near the core $x \sim 0$, solving Eqs. (28) and (29) to leading order, we obtain

$$\ell_a^{\text{II}} = \sqrt{\frac{\hbar^2}{2M(2\mu - \mathcal{D})}} \quad (48)$$

with

$$\mathcal{D} = 4(g_n + 2g_s)(c^{\text{II}} + \sqrt{n_{\pm 1}})^2 + \frac{3c^{\text{II}}\hbar^2}{(\ell^{\text{I}})^2 M(c^{\text{II}} + \kappa)}, \quad (49)$$

where c^{II} is determined by the real solution of

$$2g_n(c^{\text{II}} + \sqrt{n_{\pm 1}})^3 + \frac{c^{\text{II}}\hbar^2}{2M(\ell^{\text{I}})^2} + (q - \mu)(c^{\text{II}} + \sqrt{n_{\pm 1}}) = 0. \quad (50)$$

It is easy to check that as $g_s \rightarrow -g_n/2$, $c^{\text{II}} \rightarrow 0$, $\mathcal{D} \rightarrow 0$, and $\ell_a^{\text{II}} \rightarrow \ell_{\text{ex}}^{\text{II}}$. Consistently, the two scales we obtained indeed satisfy the working assumption $\ell_b^{\text{II}} > \ell_a^{\text{II}}$ [Fig. 5(a)]. The sign change of c^{II} across $g_s = -g_n/2$ (Fig. 5), yields a hump or a dip in $\psi_{\pm 1}$ (Fig. 6). Note that the other working assumption (i.e., $\ell_b^{\text{II}} < \ell_a^{\text{II}}$) does not lead to a consistent solution. A comparison of the two-scale *Ansatz* Eqs. (44) and (45) to numerical solutions of the GPEs is presented in Fig. 6. These results validate that this *Ansatz* effectively captures the core structure of type-II FDSs over a wide parameter regime. It is worthwhile to mention that at $q \neq 0$ stationary type-I and type-II FDSs are orthogonal, namely, the overlap $\int dx (\psi^{\text{I}})^\dagger \psi^{\text{II}} = 0$. For propagating FDSs, the overlap between the two types does not vanish and reaches the maximum value at the speed limit [23].

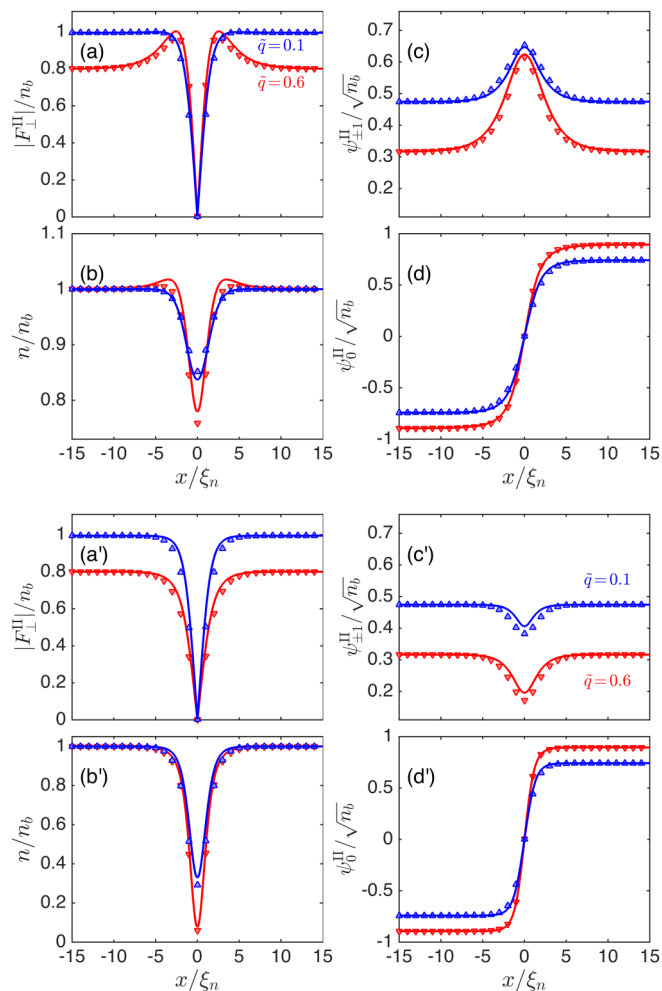


FIG. 6. A comparison between analytical predictions of type-II FDSs (solid lines) and numerical results (markers) at $\tilde{q} = 0.1$ and $\tilde{q} = 0.6$. (a), (b), (c), and (d) are for $g_s/g_n = -0.1$; (a'), (b'), (c'), and (d') are for $g_s/g_n = -0.7$.

C. Excitation energies

At $q = 0$, type-I and type-II FDSs are degenerate and are connected by a $\text{SO}(3)$ spin rotation [22]. At finite q the magnetic field breaks the $\text{SO}(3)$ rotational symmetry and the degeneracy is lifted. We can characterize the degeneracy breaking using the soliton energy [see Eq. (34)] $\delta K^{\text{I,II}} = K^{\text{I,II}} - K_g$, where $K^{\text{I,II}} = K[\psi^{\text{I,II}}]$. We find that $\delta K^{\text{I}} \leq \delta K^{\text{II}}$ and the equality is reached only when $q = 0$ (see Fig. 7).

D. Spin-singlet amplitudes

So far we have been focused on analyzing the structure of the order parameter \mathbf{F} and the mass superfluid density n which are the most relevant quantities to characterize FDSs. However, a complete description requires additional information. In general, the set $\{n, \mathbf{F}, \alpha, \delta F_z^2\}$ provides a complete description of a spin-1 BEC, where

$$\alpha \equiv \psi_0^2 - 2\psi_{+1}\psi_{-1} \quad (51)$$

is the spin-singlet amplitude and $\delta F_z^2 \equiv \psi^\dagger S_z^2 \psi = n_{+1} + n_{-1}$ couples to the quadratic Zeeman energy q [see Eq. (1)]. The

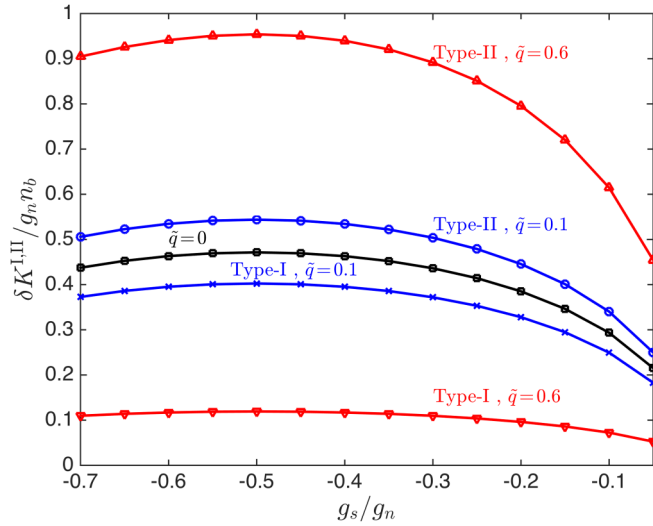


FIG. 7. Numerical results of grand canonical energies for type-I and type-II FDSs at $\tilde{q} = 0$, $\tilde{q} = 0.1$, and $\tilde{q} = 0.6$ (markers). Solid lines are guides to the eye. The soliton energy exhibits a nonmonotonic behavior as a function of g_s/g_n and the turning point occurs at the exactly solvable point $g_s/g_n = -0.5$. At $q = 0$ (black squares), type-I and type-II FDSs are degenerate as for this case their states only differ by a SO(3) spin rotation and a U(1) gauge transformation [22].

spin-singlet amplitude α is SO(2) invariant and satisfies

$$|\mathbf{F}|^2 + |\alpha|^2 = n^2. \quad (52)$$

Let us consider variations that keep \mathbf{F} , n , and δF_z^2 unchanged. Such variations appear in the phase of α . In the following we show that this particular phase change is nothing but the U(1) phase variation which is directly related to the mass current

$$\mathbf{J} = \frac{\hbar}{2Mi}(\psi^\dagger \cdot \nabla \psi - \text{H.c.}) \quad (53)$$

satisfying the continuity equation

$$\frac{\partial n}{\partial t} + \nabla \cdot \mathbf{J} = 0. \quad (54)$$

For such variations, the deformed wave functions must have the form $\tilde{\psi}_i = \psi_i e^{i\delta\theta_i(\mathbf{r})}$ and the corresponding transverse magnetization reads

$$\tilde{F}_\perp = \sqrt{2}(\psi_0 \psi_{+1}^* e^{i[\delta\theta_0(\mathbf{r}) - \delta\theta_{+1}(\mathbf{r})]} + \psi_0^* \psi_{-1} e^{i[\delta\theta_{-1}(\mathbf{r}) - \delta\theta_0(\mathbf{r})]}). \quad (55)$$

In order to keep invariant upon a global SO(2) spin rotation, namely, $\tilde{F}_\perp = e^{i\phi} F_\perp$, the condition

$$\delta\theta_0(\mathbf{r}) - \delta\theta_{+1}(\mathbf{r}) = \delta\theta_{-1}(\mathbf{r}) - \delta\theta_0(\mathbf{r}) = \phi \quad (56)$$

must be satisfied, where ϕ is an arbitrary constant phase. Phase fluctuations satisfying Eq. (56) are captured by the spin singlet, as $\tilde{\alpha} = e^{2i\delta\theta_0(\mathbf{r})}\alpha = e^{2i[\delta\theta_{+1}(\mathbf{r}) + \phi]}\alpha = e^{2i[\delta\theta_{-1}(\mathbf{r}) - \phi]}\alpha$. It is also easy to see that $\delta\theta_0(\mathbf{r})$ or $\delta\theta_{\pm 1}(\mathbf{r})$ is an overall U(1) phase variation and $\tilde{\mathbf{J}} = \mathbf{J} + n\nabla\delta\theta_0(\mathbf{r}) = \mathbf{J} + n\nabla\delta\theta_{\pm 1}(\mathbf{r})$. It is clear that a general phase variation of α does not necessarily have to be an overall U(1) phase change.

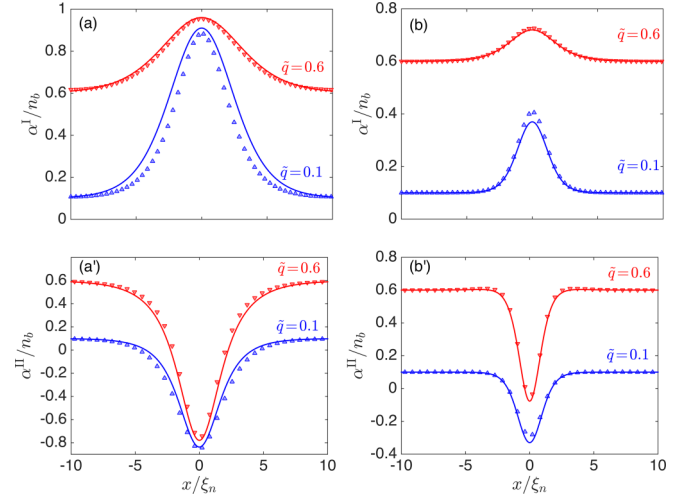


FIG. 8. Analytical predictions (solid lines) and numerical results (markers) of the spin-singlet amplitude α for type-I [(a),(b)] and type-II [(a'),(b')] FDSs at $\tilde{q} = 0.1$ and $\tilde{q} = 0.6$. (a) and (a') are for $g_s/g_n = -0.1$; (b) and (b') are for $g_s/g_n = -0.7$.

For FDSs, comparing to n , \mathbf{F} , and δF_z^2 , the spin-singlet amplitude α is a more appealing quantity to distinguish type-I from type-II FDSs as it shows a hump or a dip depending on the type (Fig. 8). The measurement of α is in the scope of the current spin-1 BECs experiments [36].

VI. NEMATIC STRUCTURE

It is sometimes useful to formulate the spin-1 BEC dynamics in terms of physical observables. The hydrodynamic formulation of the GPEs Eqs. (2) and (3) serves this purpose and provides a complete description of the condensate dynamics [37]. Such a description naturally involves nematic tensors and the corresponding currents. Although n , \mathbf{F} , α , and δF_z^2 together also fully describe a spin-1 BEC, it is not anticipated that the construction of self-contained closed dynamical equations with these variables is achievable. In this section, we explore the nematic structure of FDSs.

A. General formulation

The magnetization continuity equation reads

$$\frac{\partial F_i}{\partial t} + \nabla \cdot J_i^F = K_{iz}, \quad (57)$$

where the spin current density

$$J_i^F = \frac{\hbar}{2Mi}(\psi^\dagger S_i \nabla \psi - \nabla \psi^\dagger S_i \psi), \quad (58)$$

and the source term (or the internal current density)

$$K_{iz} = \frac{2q}{\hbar} \sum_k \epsilon_{izk} N_{zk}. \quad (59)$$

Explicitly, the components are $K_{xz} = -(2q/\hbar)N_{zy}$, $K_{yz} = (2q/\hbar)N_{zx}$, and $K_{zz} = 0$, where N_{ij} is the nematic (or quadrupolar) tensor density

$$N_{ij} = \psi^\dagger \hat{N}_{ij} \psi \quad (60)$$

with $\hat{N}_{ij} = (S_i S_j + S_j S_i)/2$ and $i, j \in \{x, y, z\}$. The nematic tensor serves as an order parameter if $F_i = 0$ [15,38] and describes spin fluctuations in the ferromagnetic phase. It is easy to recognize that $N_{zz} = \delta F_z^2$.

The nematic continuity equation reads

$$\frac{\partial N_{ij}}{\partial t} + \nabla \cdot J_{ij}^N = W_{ij} + Q_{ijz}, \quad (61)$$

where the nematic current density

$$J_{ij}^N = \frac{\hbar}{2M_i} (\psi^\dagger \hat{N}_{ij} \nabla \psi - \nabla \psi^\dagger \hat{N}_{ij} \psi), \quad (62)$$

and the source terms (or the internal current densities)

$$W_{ij} = \frac{g_s}{\hbar} \sum_{l,k} F_l (\epsilon_{ilk} N_{kj} + \epsilon_{jlk} N_{ki}), \quad (63)$$

$$Q_{ijz} = \frac{q}{2\hbar} \sum_k F_k (\epsilon_{izk} \delta_{zj} + \epsilon_{jzk} \delta_{zi}). \quad (64)$$

Since $\text{Tr}N = \sum_i N_{ii} = n$, the total density continuity equation (54) can be obtained by taking the trace of Eq. (61). It is easy to see that $\text{Tr}W = 0$ and $Q_{iiz} = 0$. Also $Q_{xzz} = Q_{zxx} = -(q/2\hbar)F_y$ and $Q_{yzz} = Q_{zzy} = (q/2\hbar)F_x$, and all the other components are zero. Hence Q_{ijz} does not contain new information. The continuity equations (54), (57), (61) and the equation of motion of the mass current \mathbf{J} (Euler equation) together provide a complete description of spin-1 BECs dynamics [37].

Except the total number density n and the total number current \mathbf{J} , the expressions of other densities and currents vary when applying spin rotations. Hence it is useful to construct rotationally invariant quantities to reveal intrinsic currents. Here we find that the densities

$$F \equiv \left[\sum_i (F_i)^2 \right]^{1/2}, \quad \mathcal{N} \equiv \left[\sum_{ij} (N_{ij})^2 \right]^{1/2} \quad (65)$$

and the current densities

$$\mathcal{J}_F \equiv \left[\sum_i (J_i^F)^2 \right]^{1/2}, \quad \mathcal{J}_N \equiv \left[\sum_{ij} (J_{ij}^N)^2 \right]^{1/2},$$

$$\mathcal{W} \equiv \left[\sum_{ij} (W_{ij})^2 \right]^{1/2} \quad (66)$$

are invariant under SO(3) spin rotations. The source terms

$$\mathcal{Q} \equiv \left[\sum_{ij} (Q_{ijz})^2 \right]^{1/2}, \quad \mathcal{K} \equiv \left[\sum_i (K_{iz})^2 \right]^{1/2} \quad (67)$$

only appear in the equation of motion when $q \neq 0$, and are SO(2) rotationally invariant.

B. Nematic structure of FDSs

At the exactly solvable point $g_s = -g_n/2$, the invariant nematic densities read

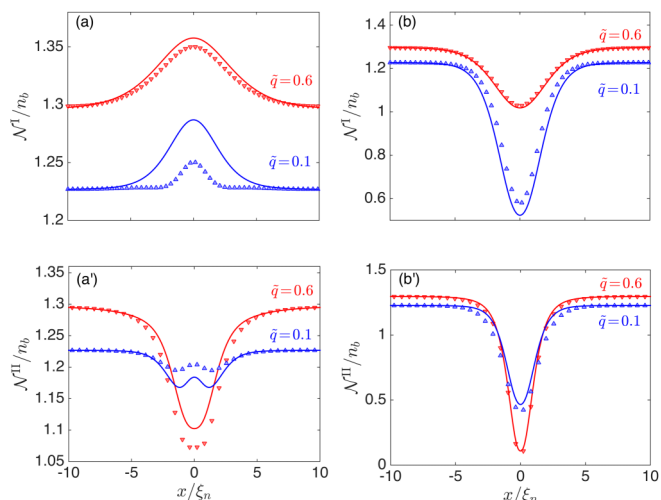


FIG. 9. Analytical predictions (solid lines) and numerical results (markers) of the rotationally invariant nematic density \mathcal{N} for type-I [(a),(b)] and type-II [(a'),(b')] FDSs at $\tilde{q} = 0.1$ and $\tilde{q} = 0.6$. (a) and (a') are for $g_s/g_n = -0.1$; (b) and (b') are for $g_s/g_n = -0.7$.

$$(\mathcal{N}^{I,II})^2 = \frac{1}{4} \left[4 \left(n_b - \frac{g_n n_b \mp q}{g_n \cosh\left(\frac{x}{\ell_{I,II}}\right) + g_n} \right)^2 + \left(n_b \mp \frac{q}{g_n} \right)^2 \tanh^4\left(\frac{x}{2\ell_{I,II}}\right) + \left(n_b \pm \frac{q}{g_n} \right)^2 \right], \quad (68)$$

where the upper (lower) sign in front of q specifies the type-I (type-II) FDS. Away from the exactly solvable point, the *Ansätze* also describe well the nematic densities in a wide range parameter regime (Fig. 9).

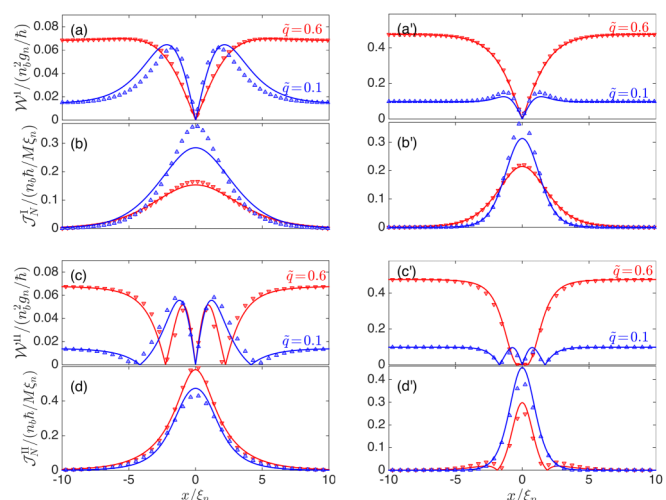


FIG. 10. Profiles of invariant internal currents of FDSs. Analytical predictions (solid lines) and numerical results (markers) are shown at $\tilde{q} = 0.1$ (blue) and $\tilde{q} = 0.6$ (red). (a), (b), (c), and (d) are for $g_s/g_n = -0.1$; (a'), (b'), (c'), and (d') are for $g_s/g_n = -0.7$. The y-axis labels of (a'), (b'), (c'), and (d') are the same as the y-axis labels of (a), (b), (c), and (d).

Figure 10 shows the profiles of the invariant internal current densities. At the exactly solvable point,

$$(\mathcal{J}_N^{I,II})^2 = \frac{\hbar^2(g_n^2 n_b^2 - q^2)}{32(\ell_q^{I,II})^2 M^2 g_n^2} \operatorname{sech}^4\left(\frac{x}{2\ell_q^{I,II}}\right), \quad (69)$$

$$(\mathcal{W}^{I,II})^2 = \frac{g_n^2 n_b^2 - q^2}{8g_n^2 \hbar^2} \tanh^2\left(\frac{x}{2\ell_q^{I,II}}\right) \times \operatorname{sech}^4\left(\frac{x}{2\ell_q^{I,II}}\right) \left[g_n n_b \pm q \cosh\left(\frac{x}{2\ell_q^{I,II}}\right) \right]^2, \quad (70)$$

here the plus sign and minus sign in front of q specify type-I and type-II FDSs, respectively.

VII. CONCLUSION AND DISCUSSION

We have studied the \mathbb{Z}_2 topological defects in the easy-plane phase of a ferromagnetic spin-1 BEC. We propose analytical *Ansätze* to describe FDSs which are the defects in the magnetic order. The *Ansätze* reduce to the exact solutions at the exactly solvable point and show good agreement with numerical results over the whole easy-plane phase. The width of type-I FDSs is captured by a single scale while the core structure of type-II FDSs require two scales. Moreover, exact DDD vector solitons, which are the \mathbb{Z}_2 defects in the mass superfluid order, are also presented. FDSs are expected to play an important role in late time dynamics of 1D quenches [26,27] and equilibrium properties at finite temperature [39].

Experimental advances now allow plane-confined BECs with flat-bottom traps [40,41] and the measurement of transverse magnetic structures by the nondestructive imaging method [36,42], opening the possibility for detailed experimental investigations of FDSs. The so-called magnetic phase imprinting method, which has been used to experimentally create pairs of magnetic solitons [43,44], could be a suitable method to create FDSs in a ferromagnetic spin-1 BEC. Very recently, the easy-plane phase of a homogeneous ferromagnetic spin-1 BEC has been prepared in a flat-bottom trapped quasi-one-dimensional system [39]. The magnetic phase imprinting method applies circularly polarized light to imprint a phase shift of $\pm\pi$ onto two $m = \pm 1$ hyperfine components on half the system by using a magnetic shadow [43,44]. This hence realizes a π spin rotation of the transverse magnetization of half of the system, seeding the key ingredient of a single FDS.

In this paper we focus on kinks/topological solitons in the easy-plane phase of ferromagnetic spin-1 BECs. A FDS is a \mathbb{Z}_2 topological defect which interpolates between oppositely magnetized domains. From another perspective, it could be useful to view FDSs as members of the soliton family in spin-1 BECs and compare them with other nonlinear waves. Here we give a brief summary of the main focus of recent soliton studies in spin-1 BECs. The list is incomplete; for instance, solitons in systems with optical lattices and dipole-dipole interactions [45,46] are not included. Also we only consider systems with the finite background density, i.e., the positive density-dependent interaction strength. According to the terminologies, there are mainly two varieties. (i) *Vector solitons*: each component has either dark or bright soliton structure

[47–52] (Ref. [52] discusses two-dimensional extensions of such excitations, i.e., vortex-bright structures). Various vector solitons in a 1D harmonically trapped spin-1 system have been recently summarized in Ref. [32]. Vector solitons may or may not correspond to topological structures in the order parameter. There are two interesting examples which are topological. One is the dark-dark-dark vector soliton in ferromagnetic BECs which is the topological defect in the mass superfluid order as discussed in Sec. IV. Another one is the bright-dark-bright vector soliton in an antiferromagnetic BEC which manifests itself as a domain wall in the spin director field (the order parameter) [53]. (ii) *Magnetic solitons*: this soliton was initially introduced in miscible two-component BECs [54] and can be embedded into an antiferromagnetic spin-1 BEC in the absence of a magnetic field [43,44,55]. One important aspect of this soliton is that it is an analytical solution which is beyond the Manakov limit. The solution is obtained with the constant density approximation which works well for weak spin-dependent coupling g_s . In the context of two-component BECs, it emphasizes that there is no bright or dark soliton structure in the components, while the pseudomagnetization F_z shows a bright soliton structure. When embedding into antiferromagnetic spin-1 BECs, its configuration varies under SO(3) spin rotations [55] as what happens for FDSs at the $q \rightarrow 0$ limit [22]. The magnetic soliton is not a topological soliton as there is no invariant topological charge associated with it (neither in its original two-component formulation nor in its realizations in an antiferromagnetic spin-1 BEC). FDSs do not belong to vector solitons, as not all the components of FDSs have bright or dark soliton structure. The topological nature of FDSs also clearly distinguish themselves from magnetic solitons. Moreover, exact solutions for FDSs are available at a strong spin-dependent interaction coupling ($g_s/g_n = -1/2$) [22,23] which is far beyond the Manakov limit ($g_s = 0$ in the context of spin-1 BECs).

FDSs are Ising-type magnetic domain walls. A natural question is whether Bloch-type and Néel-type magnetic domain walls could exist in the easy-plane phase. A Néel-type-like domain wall has been investigated numerically in a trapped 1D ferromagnetic BEC at $q = 0$ [56], which might be related to the wall defects appearing transiently in early quench dynamics from unmagnetized or partially magnetized states [25,57]. However it is not clear whether the trap potential plays the key role to sustain this structure. Searching for Bloch-type and Néel-type magnetic domain walls in the easy-plane phase of ferromagnetic BECs deserves future investigations.

So far we only consider excitations from a uniform ground state. In immiscible condensates, domain walls are also referred to as the interfaces between the spatially separated components of the condensate; examples are density (or pseudomagnetization F_z) domain walls in immiscible binary BECs [58–61], and magnetic domain walls in ferromagnetic spin-1 BECs for a negative quadratic Zeeman shift $q < 0$ [62].

ACKNOWLEDGMENTS

X.Y. acknowledges the support from NSAF with Grant No. U1930403 and NSFC with Grant No. 12175215. P.B.B. acknowledges support from the Marsden Fund of the Royal Society of New Zealand.

- [1] T.-L. Ho, Spinor Bose Condensates in Optical Traps, *Phys. Rev. Lett.* **81**, 742 (1998).
- [2] T. Ohmi and K. Machida, Bose-Einstein condensation with internal degrees of freedom in alkali atom gases, *J. Phys. Soc. Jpn.* **67**, 1822 (1998).
- [3] J. Stenger, S. Inouye, D. M. Stamper-Kurn, H. J. Miesner, A. P. Chikkatur, and W. Ketterle, Spin domains in ground-state Bose-Einstein condensates, *Nature (London)* **396**, 345 (1998).
- [4] L. E. Sadler, J. M. Higbie, S. R. Leslie, M. Vengalattore, and D. M. Stamper-Kurn, Spontaneous symmetry breaking in a quenched ferromagnetic spinor Bose-Einstein condensate, *Nature (London)* **443**, 312 (2006).
- [5] D. M. Stamper-Kurn and M. Ueda, Spinor Bose gases: Symmetries, magnetism, and quantum dynamics, *Rev. Mod. Phys.* **85**, 1191 (2013).
- [6] Y. Kawaguchi and M. Ueda, Spinor Bose-Einstein condensates, *Phys. Rep.* **520**, 253 (2012).
- [7] A. J. A. James and A. Lamacraft, Phase Diagram of Two-Dimensional Polar Condensates in a Magnetic Field, *Phys. Rev. Lett.* **106**, 140402 (2011).
- [8] M. Kobayashi, Berezinskii-Kosterlitz-Thouless transition of spin-1 spinor Bose gases in the presence of the quadratic Zeeman effect, *J. Phys. Soc. Jpn.* **88**, 094001 (2019).
- [9] H. Saito, Y. Kawaguchi, and M. Ueda, Kibble-Zurek mechanism in a quenched ferromagnetic Bose-Einstein condensate, *Phys. Rev. A* **76**, 043613 (2007).
- [10] B. Damski and W. H. Zurek, Dynamics of a Quantum Phase Transition in a Ferromagnetic Bose-Einstein Condensate, *Phys. Rev. Lett.* **99**, 130402 (2007).
- [11] A. Lamacraft, Quantum Quenches in a Spinor Condensate, *Phys. Rev. Lett.* **98**, 160404 (2007).
- [12] S. Mukerjee, C. Xu, and J. E. Moore, Dynamical models and the phase ordering kinetics of the $s = 1$ spinor condensate, *Phys. Rev. B* **76**, 104519 (2007).
- [13] L. A. Williamson and P. B. Blakie, Universal Coarsening Dynamics of a Quenched Ferromagnetic Spin-1 Condensate, *Phys. Rev. Lett.* **116**, 025301 (2016).
- [14] L. A. Williamson and P. B. Blakie, Coarsening Dynamics of an Isotropic Ferromagnetic Superfluid, *Phys. Rev. Lett.* **119**, 255301 (2017).
- [15] L. M. Symes and P. B. Blakie, Nematic ordering dynamics of an antiferromagnetic spin-1 condensate, *Phys. Rev. A* **96**, 013602 (2017).
- [16] C.-M. Schmied, T. Gasenzer, and P. B. Blakie, Violation of single-length-scaling dynamics via spin vortices in an isolated spin-1 Bose gas, *Phys. Rev. A* **100**, 033603 (2019).
- [17] A. Bourges and P. B. Blakie, Different growth rates for spin and superfluid order in a quenched spinor condensate, *Phys. Rev. A* **95**, 023616 (2017).
- [18] R. Barnett, A. Polkovnikov, and M. Vengalattore, Prethermalization in quenched spinor condensates, *Phys. Rev. A* **84**, 023606 (2011).
- [19] K. Fujimoto, R. Hamazaki, and M. Ueda, Flemish Strings of Magnetic Solitons and a Nonthermal Fixed Point in a One-Dimensional Antiferromagnetic Spin-1 Bose Gas, *Phys. Rev. Lett.* **122**, 173001 (2019).
- [20] L. A. Williamson and P. B. Blakie, Dynamics of polar-core spin vortices in a ferromagnetic spin-1 Bose-Einstein condensate, *Phys. Rev. A* **94**, 063615 (2016).
- [21] A. M. Turner, Mass of a Spin Vortex in a Bose-Einstein Condensate, *Phys. Rev. Lett.* **103**, 080603 (2009).
- [22] X. Yu and P. B. Blakie, Dark-soliton-like magnetic domain walls in a two-dimensional ferromagnetic superfluid, *Phys. Rev. Research* **3**, 023043 (2021).
- [23] X. Yu and P. B. Blakie, Propagating Ferrodark Solitons in a Superfluid: Exact Solutions and Anomalous Dynamics, *Phys. Rev. Lett.* **128**, 125301 (2022).
- [24] H. Saito, Y. Kawaguchi, and M. Ueda, Topological defect formation in a quenched ferromagnetic Bose-Einstein condensates, *Phys. Rev. A* **75**, 013621 (2007).
- [25] H. Saito and M. Ueda, Spontaneous magnetization and structure formation in a spin-1 ferromagnetic Bose-Einstein condensate, *Phys. Rev. A* **72**, 023610 (2005).
- [26] M. Prüfer, P. Kunkel, H. Strobel, S. Lannig, D. Linnemann, C.-M. Schmied, J. Berges, T. Gasenzer, and M. K. Oberthaler, Observation of universal dynamics in a spinor Bose gas far from equilibrium, *Nature (London)* **563**, 217 (2018).
- [27] C.-M. Schmied, M. Prüfer, M. K. Oberthaler, and T. Gasenzer, Bidirectional universal dynamics in a spinor Bose gas close to a nonthermal fixed point, *Phys. Rev. A* **99**, 033611 (2019).
- [28] T. Mizushima, K. Machida, and T. Kita, Mermin-Ho Vortex in Ferromagnetic Spinor Bose-Einstein Condensates, *Phys. Rev. Lett.* **89**, 030401 (2002).
- [29] K. Kudo and Y. Kawaguchi, Coarsening dynamics driven by vortex-antivortex annihilation in ferromagnetic Bose-Einstein condensates, *Phys. Rev. A* **91**, 053609 (2015).
- [30] W. Zhang, S. Yi, and L. You, Mean field ground state of a spin-1 condensate in a magnetic field, *New J. Phys.* **5**, 77 (2003).
- [31] S. J. Huh, K. Kim, K. Kwon, and J.-Y. Choi, Observation of a strongly ferromagnetic spinor Bose-Einstein condensate, *Phys. Rev. Research* **2**, 033471 (2020).
- [32] G. C. Katsimiga, S. I. Mistakidis, P. Schmelcher, and P. G. Kevrekidis, Phase diagram, stability and magnetic properties of nonlinear excitations in spinor Bose-Einstein condensates, *New J. Phys.* **23**, 013015 (2021).
- [33] No convergent DDD soliton solution is found for $|g_s/g_n| < 0.1$.
- [34] F. Y. Lim and W. Bao, Numerical methods for computing the ground state of spin-1 Bose-Einstein condensates in a uniform magnetic field, *Phys. Rev. E* **78**, 066704 (2008).
- [35] W. Bao and F. Y. Lim, Computing ground states of spin-1 Bose-Einstein condensates by the normalized gradient flow, *SIAM J. Sci. Comput.* **30**, 1925 (2008).
- [36] P. Kunkel, M. Prüfer, S. Lannig, R. Rosa-Medina, A. Bonnin, M. Gärtner, H. Strobel, and M. K. Oberthaler, Simultaneous Readout of Noncommuting Collective Spin Observables beyond the Standard Quantum Limit, *Phys. Rev. Lett.* **123**, 063603 (2019).
- [37] E. Yukawa and M. Ueda, Hydrodynamic description of spin-1 Bose-Einstein condensates, *Phys. Rev. A* **86**, 063614 (2012).
- [38] E. F. Gramsbergen, L. Longa, and W. H. de Jeu, Landau theory of the nematic-isotropic phase transition, *Phys. Rep.* **135**, 195 (1986).
- [39] M. Prüfer, D. Spitz, S. Lannig, H. Strobel, J. Berges, and M. K. Oberthaler, Condensation and thermalization of an easy-plane ferromagnet in a spinor Bose gas, [arXiv:2205.06188](https://arxiv.org/abs/2205.06188).
- [40] L. Chomaz, L. Corman, T. Bienaimé, R. Desbuquois, C. Weitenberg, S. Nascimbène, J. Beugnon, and J. Dalibard, Emergence of coherence via transverse condensation in a

- uniform quasi-two-dimensional Bose gas, *Nat. Commun.* **6**, 6162 (2015).
- [41] G. Gauthier, I. Lenton, N. McKay Parry, M. Baker, M. J. Davis, H. Rubinsztein-Dunlop, and T. W. Neely, Direct imaging of a digital-micromirror device for configurable microscopic optical potentials, *Optica* **3**, 1136 (2016).
- [42] J. M. Higbie, L. E. Sadler, S. Inouye, A. P. Chikkatur, S. R. Leslie, K. L. Moore, V. Savalli, and D. M. Stamper-Kurn, Direct Nondestructive Imaging of Magnetization in a Spin-1 Bose-Einstein Gas, *Phys. Rev. Lett.* **95**, 050401 (2005).
- [43] A. Farolfi, D. Trypogeorgos, C. Mordini, G. Lamporesi, and G. Ferrari, Observation of Magnetic Solitons in Two-Component Bose-Einstein Condensates, *Phys. Rev. Lett.* **125**, 030401 (2020).
- [44] X. Chai, D. Lao, K. Fujimoto, R. Hamazaki, M. Ueda, and C. Raman, Magnetic Solitons in a Spin-1 Bose-Einstein Condensate, *Phys. Rev. Lett.* **125**, 030402 (2020).
- [45] Z.-W. Xie, W. Zhang, S. T. Chui, and W. M. Liu, Magnetic solitons of spinor Bose-Einstein condensates in an optical lattice, *Phys. Rev. A* **69**, 053609 (2004).
- [46] Z. D. Li, P. B. He, L. Li, J. Q. Liang, and W. M. Liu, Magnetic soliton and soliton collisions of spinor Bose-Einstein condensates in an optical lattice, *Phys. Rev. A* **71**, 053611 (2005).
- [47] H. E. Nistazakis, D. J. Frantzeskakis, P. G. Kevrekidis, B. A. Malomed, and R. Carretero-González, Bright-dark soliton complexes in spinor Bose-Einstein condensates, *Phys. Rev. A* **77**, 033612 (2008).
- [48] Th. Busch and J. R. Anglin, Dark-Bright Solitons in Inhomogeneous Bose-Einstein Condensates, *Phys. Rev. Lett.* **87**, 010401 (2001).
- [49] X. Liu, H. Pu, B. Xiong, W. M. Liu, and J. Gong, Formation and transformation of vector solitons in two-species Bose-Einstein condensates with a tunable interaction, *Phys. Rev. A* **79**, 013423 (2009).
- [50] T. M. Bersano, V. Gokhroo, M. A. Khomehchi, J. D'Ambroise, D. J. Frantzeskakis, P. Engels, and P. G. Kevrekidis, Three-Component Soliton States in Spinor $f = 1$ Bose-Einstein Condensates, *Phys. Rev. Lett.* **120**, 063202 (2018).
- [51] S. Lannig, C.-M. Schmied, M. Prüfer, P. Kunkel, R. Strohmaier, H. Strobel, T. Gasenzer, P. G. Kevrekidis, and M. K. Oberthaler, Collisions of Three-Component Vector Solitons in Bose-Einstein Condensates, *Phys. Rev. Lett.* **125**, 170401 (2020).
- [52] G. C. Katsimiga, S. I. Mistakidis, K. Mukherjee, P. G. Kevrekidis, and P. Schmelcher, Stability and dynamics across magnetic phases of nonlinear excitations in two-dimensional spinor Bose-Einstein condensates, [arXiv:2109.07404](https://arxiv.org/abs/2109.07404).
- [53] S. Kang, S. W. Seo, H. Takeuchi, and Y. Shin, Observation of Wall-Vortex Composite Defects in a Spinor Bose-Einstein Condensate, *Phys. Rev. Lett.* **122**, 095301 (2019).
- [54] C. Qu, L. P. Pitaevskii, and S. Stringari, Magnetic Solitons in a Binary Bose-Einstein Condensate, *Phys. Rev. Lett.* **116**, 160402 (2016).
- [55] X. Chai, D. Lao, K. Fujimoto, and C. Raman, Magnetic soliton: From two to three components with SO(3) symmetry, *Phys. Rev. Research* **3**, L012003 (2021).
- [56] W. Zhang, Ö. E. Müstecaplıoğlu, and L. You, Solitons in a trapped spin-1 atomic condensate, *Phys. Rev. A* **75**, 043601 (2007).
- [57] W. Zhang, D. L. Zhou, M.-S. Chang, M. S. Chapman, and L. You, Dynamical Instability and Domain Formation in a Spin-1 Bose-Einstein Condensate, *Phys. Rev. Lett.* **95**, 180403 (2005).
- [58] P. Ao and S. T. Chui, Binary Bose-Einstein condensate mixtures in weakly and strongly segregated phases, *Phys. Rev. A* **58**, 4836 (1998).
- [59] S. Coen and M. Haelterman, Domain Wall Solitons in Binary Mixtures of Bose-Einstein Condensates, *Phys. Rev. Lett.* **87**, 140401 (2001).
- [60] X. Chai, L. You, and C. Raman, Magnetic solitons in an immiscible two-component Bose-Einstein condensate, *Phys. Rev. A* **105**, 013313 (2022).
- [61] In Ref. [60], when the distance between two domain walls is small, the two-wall structure looks like a single soliton.
- [62] H. Takeuchi, Spin-current instability at a magnetic domain wall in a ferromagnetic superfluid: A generation mechanism of eccentric fractional skyrmions, *Phys. Rev. A* **105**, 013328 (2022).